Mare Basalt, Touchstone

70215

8110 grams

DRAFT

Figure 1: Close-up of surface of 70215,261 showing zap pits and apparent vugs. Sample is about 12 cm long. NASA # S89-34498.

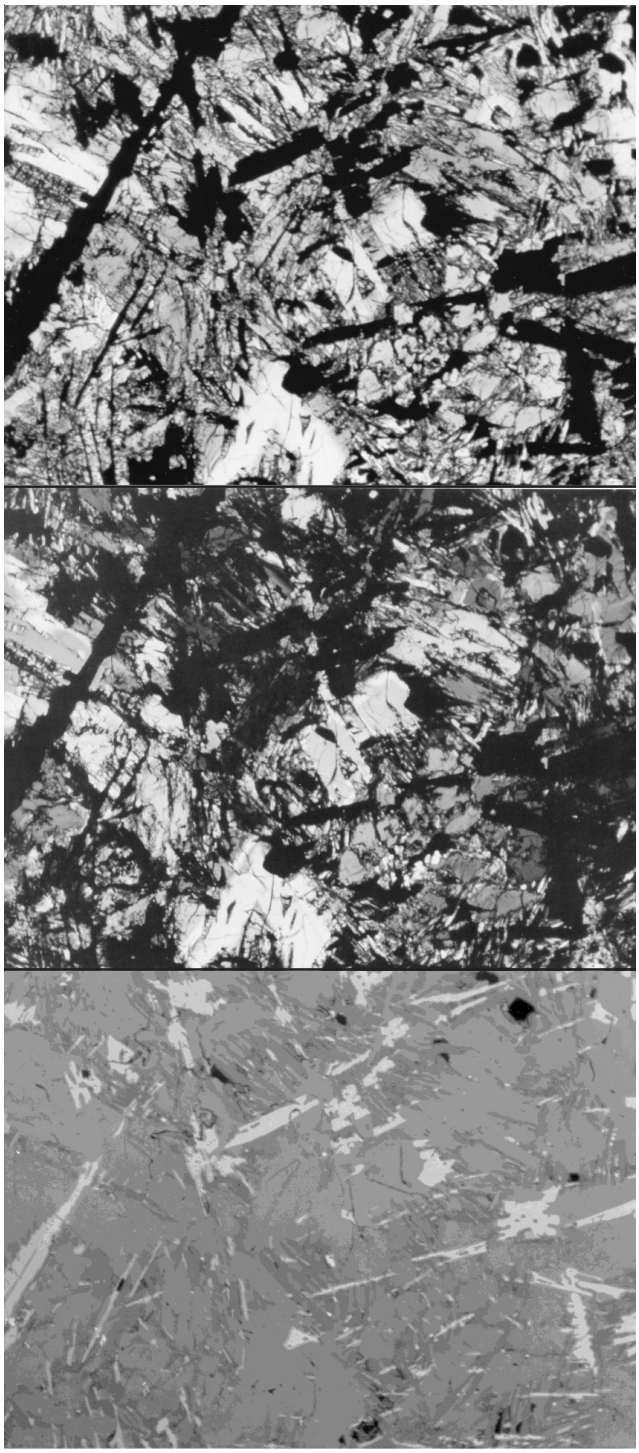

Figure 2: Photomicrographs of thin section 70215,89 (field of view 1.3 mm). Top = plane polarized light, middle = crossed-nicols, bottom = reflected). NASA # S79-26738-26740. Olivine is clear, surrounded by colored pyroxene. Ilmenite is opaque with high reflectivity. Plagioclase is interstitial, with low reflectivity.

Introduction

Did you ever want to reach out and touch the Moon? Here's your chance. Lunar sample 70215 is a dense, fine-grained porphyritic mare basalt that has been used to create "touchstones" for public display (*see list under Processing*). It was collected about 60 m from the Lunar Module and is one of the largest stones returned from the Moon.

Neal and Taylor (1993) catalogued 70215 as a "high-Ti, Mare Basalt" and it contains an abundance of ilmenite (~13%). It has been dated by Kirsten and Horn (1974) at 3.84 ± 0.04 b.y.

70215 was found sitting on the surface and has micrometeorite craters on all faces. It contained small vugs with projecting plates of ilmenite and pyroxene (figure 1). 70215 has been used for numerous scientific experiments, including experimental petrology, physical properties and magnetic properties. A sizeable portion of the rock remains available for additional studies.

Petrography

Wilshire (in Apollo 17 Lunar Sample Catalog), Longhi et al. (1974), Dymek et al. (1975), Brown et al. (1975), McGee et al. (1977) and Neal and Taylor (1993) gave various descriptions of 70215. It has variously been termed a "fine-grained, subvariolitic basalt", "spherulitic, fine-grained high-Ti basalt", "Type 1A, Apollo 17 high-Ti basalt", "fine-grained porphyritic basalt" and "medium dark gray, fine-grained basalt". Walker et al. (1976) and McGee et al. (1977) noted that there were distinctly different textural regions in thin sections of 70215. Walker et al. simply termed these "grainy" and "fuzzy" regions and noted a slight (but significant) variation in bulk composition. The contact between the regions is gradational, but can be seen in thin sections ,145 and ,147. Both regions contain a small amount of irregular pore space and rare vesicles 0.05 to 0.1 mm in diameter. Figure 2 shows the texture of one region. The reason for a variation in texture (and composition) in this rock has not been explained.

McGee et al. (1977) describe the finer-grained region consisting of "phenocrysts of olivine and ilmenite in a groundmass of fan-shaped intergrowths of plagioclase and pyroxene. The olivine displays a variety of shapes including elongate, hollow prisms (0.1x0.4 to 0.2x0.8mm), equant and subequant grains (0.1-0.3mm)

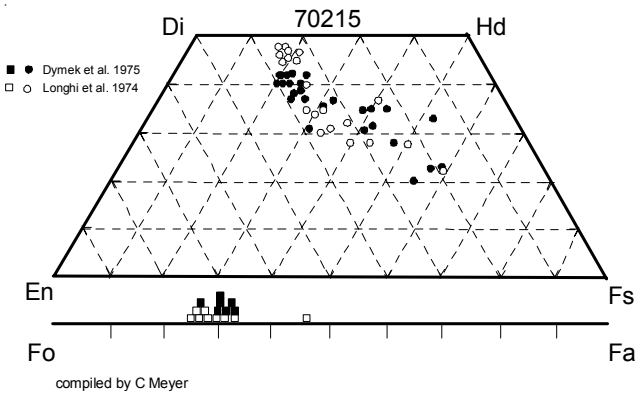

Figure 3: Pyroxene and olivine composition in 70215 (adapted from Longhi et al. 1974 and Dymek et al. 1975).

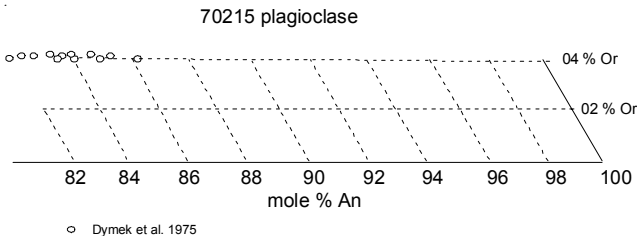

Figure 4: Plagioclase composition in 70215 (from Dymek et al. 1975).

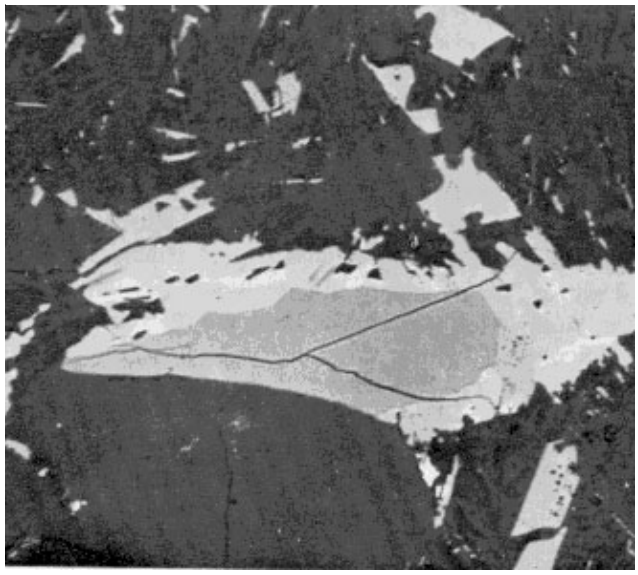

Figure 5: An armalcolite grain adjacent to olivine grain in 70215,159, illustrating the reaction relationship of armalcolite with the melt, forming ilmenite with rutile exsolution. The armacolite grains was protected on one side by the attached olivine. Grain is about 100 microns across. Picture from El Goresy et al. (1974).

and skeletal, euhedral phenocrysts (0.1-0.3mm). Ilmenite phenocrysts occur as equant grains (0.4mm) and as laths (0.6-2.0mm) with irregular jagged edges which commonly contain cores of armalcolite and lamellae of rutile." The matrix contains minute (0.3mm) "bow-tie" intergrowths of plagioclase and pyroxene along with needle-like laths of ilmenite. Olivine phenocyrsts contain small octahedra of Cr-ulvöspinel.

McGee et al. (1977) describe the coarser-grained region consisting of "equal size olivine and pyroxene phenocrysts (0.3-0.8mm) set in a matrix consisting of feathery to acicular intergrowths of subparrallel plagioclase and pyroxene crystals. Olivine phenocrysts are epitaxially overgrown with pyroxene. Rare anhedral grains of plagioclase are present. Skeletal laths of ilmenite (0.01-0.08mm) are commonly arranged in parallel sets which display optical continuity. Lamallae of rutile are common in ilmenite." Troilite and native iron occur in the matrix".

At low pressure, olivine and armalcolite were the first phases to crystallize during cooling of the 70215 lava (figure 6). On further cooling, these first-forming phases partially reacted with the melt to form clinopyroxene and ilmenite (figure 5). Rapid cooling apparently prevented early plagioclase nucleation, with Ca and Al being used up in the pyroxene, before plagioclase finally joined the crystallization sequence

Mineralogical Mode 70215

	Longhi et al. 1974	Dymek et al. 1975	McGee et al. 1977	Brown et al. 1975
Olivine	7 %	6	6-9	9.2
Pyroxene	42	58	41-58	41
Plagioclase	29	18	13-29	12.8
Opaques	18			37
Ilmenite		13	13-37	
Chromite + Usp.				
Silica mesostasis	4	4	4	

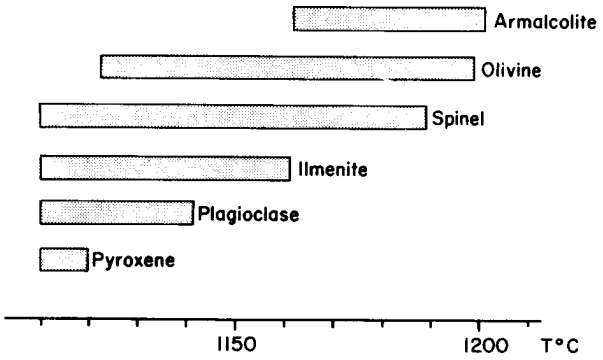

Figure 6: Low pressure crystallization sequence for 70215 (from Kesson 1975).

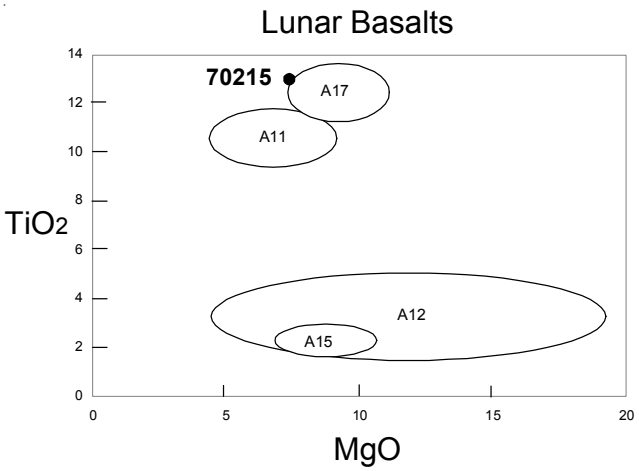

Figure 7: Composition of 70215 compared with that of other lunar basalts.

(Dymek et al. 1975). Mesostasis contains silica (4%) and K-rich glass.

Neal et al. (1990) updated the chemical classification of Apollo 17 basalts originally proposed by Rhodes et al. (1976) and classified 70215 as type high-Ti, B2. It can be related to other Apollo 17 basalts by factional crystallization in the source region and/or near surface fractionation of olivine, Cr-spinel and/or ilmenite (Walker et al. 1975, Neal and Taylor 1992).

Mineralogy

Olivine: Olivine phenocrysts in 70215 show the effect of "rapid crystallization, being poorly formed, hollow, and skeletal in habit" (Dymek et al. 1975). Olivine ($Fo_{75\text{-}65}$) contains only minor amount of "trace elements".

Pyroxene: Pink pyroxene typically occurs as reaction rims on olivine. It is high in Ca ($Wo_{37\text{-}44}$) and in minor elements (Al, Ti, Cr). Groundmass pyroxene is more iron rich (figure 3).

Plagioclase: Plagioclase in 70215 is found as intergrowths with Fe-rich pyroxene, often in 'bowtie' spherulite textures. It is relatively sodic $An_{86\text{-}80}$ (figure 4).

Armalcolite: Rare armalcolite is found in cores of large ilmenite (figure 5).

Ilmenite: Ilmenite replaced armalcolite by reaction with the melt. Muhich et al. (1990) reported variations in ilmenite composition, partially due to rutile exsolution.

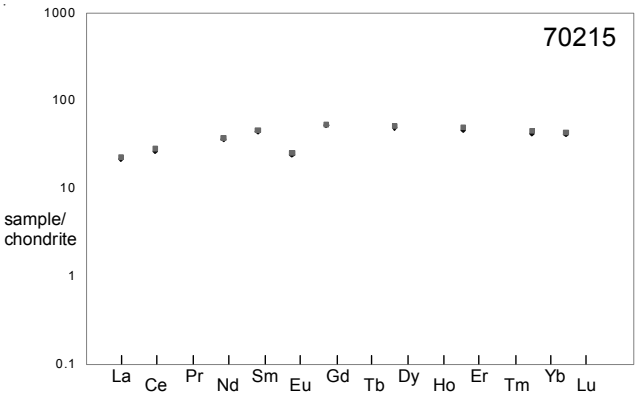

Figure 8: Normalized rare-earth-element composition diagram for 70215 (data from Shih et al. 1975 and Masuda et al. 1974).

Cr-ulvöspinel: Cr-ulvöspinel occurs as small octahedra in olivine and pyroxene phenocrysts (Dymek et al. 1975).

Chemistry

The chemical composition of 70215 has been determined by LSPET (1973), Rhodes et al. (1974), Shih et al. (1975), Wanke et al. (1975), Duncan et al. (1974), Rose et al. (1974), Masuda (1974) Dickinson et al. (1989) and Brunfelt et al. (1974) (Table 1). The high TiO_2 content (~ 13 wt. %) is typical of Apollo 17 basalts (figure 7). The light REE are significantly depleted (figure 8) indicating that the source region was already evolved (Shaffer et al. 1990).

Gibson et al. (1974, 1975, 1976), Moore et al. (1974) and Petrowski et al. (1974) reported 2210, 2040 and 1689 ppm S (respectively); Garg and Ehmann (1976) reported 214 ppm Zr and 6.8 ppm Hf; Hughes and

Schmitt (1985) reported 6.2 ppm Hf; Muller (1976), Moore and Lewis (1976) and Goel et al. (1975) reported 3, 88 and 20 ppm N (respectively); and Moore and Lewis (1976) reported 31 ppm C.

Radiogenic age dating

Nyquist et al. (1976) tried to date 70215 by Rb-Sr, but couldn't obtain a wide enough spread in Rb-Sr to obtain an age. Kirsten and Horn (1974) determined a Ar/Ar plateau age of 3.84 ± 0.04 b.y. (figure 9). Schaeffer et al. (1977) used a laser to obtain numerous Ar/Ar ages of minerals and intergrowths in 70215 ranging from ~3.6 b.y. for olivine to ~3.8 b.y. for intrgrowths.

Cosmogenic isotopes and exposure ages

Kirsten and Horn (1974) determined a cosmic ray exposure age of 100 ± 12 m.y. with the ^{38}Ar and Drozd et al. (1977) reported a Kr-Kr exposure age of 126 ± 3 m.y. which they attribute to the age of Camelot Crater.

Other Studies

Longhi et al. (1974), Kesson (1975), Green et al. (1975), O'Hara and Humphries (1975) and Walker et al. (1976) attempted to determine the depth of origin of high-Ti basalts by performing high pressure experiments on 70215 and synthetic compositions (figures 10-13). The slight variation in starting composition, along with experimental details, led to considerable discussion (see Walker et al., Kesson and Ringwood 1976).

The remanent magnetism of 70215 was studied by Runcorn et al. (1974), Nagata et al. (1974), Pearce et al. (1974), Sugiura and Strangeway (1980), Hargarves and Dorety (1975), Cisowski et al. (1977), Collinson et al. (1975), Stephenson et al. (1974, 1975) and others (figure 18).

Mizutani and Osako (1974) determined seismic wave velocities as a function of pressure of 70215. They also reported thermal diffusivities. Warren et al. (1974) and Tittman et al. (1975, 1976 and 1978) studied the effect of adsorbed volatiles upon the attenuation of ultrasound in 70215. Ahrens et al. (1977) used pieces of 70215 to study the shock compression alteration of the dynamic properties of the lunar surface.

Processing

Sample 70215 broke into two subequal pieces (,3 and ,4) (figure 14). Two slabs were cut from ,4 (figures 15-17) leading to many allocations. There are a total of 25 thin sections.

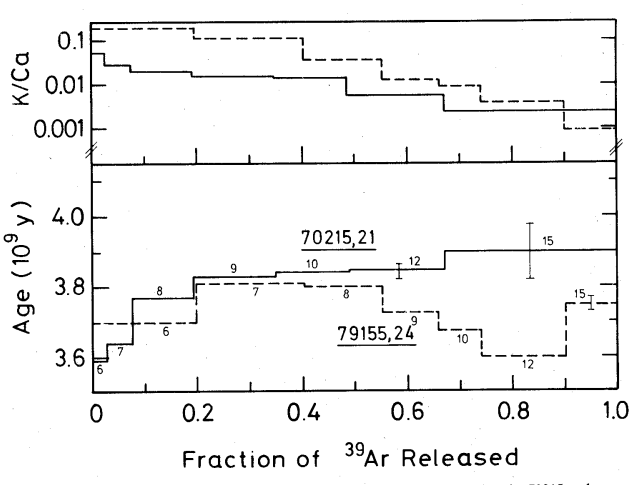

Figure 9: Argon 39/40 release pattern for 70215 and 79155 (from Kirsten and Horn 1974).

Summary of Age Data for 70215

	Ar/Ar
Kirsten and Horn 1974	3.84 ± 0.04 b.y.
Schaffer et al. 1977	3.63 - 3.85

Touchstones	,238	Space Center Houston
	,287	Kennedy Space Center
	,84	Smithsonian Air and Space
	,286	Mexico City
	,263	Vancouver, BC
Display	,93	Alamogordo, NM

List of Photo #s for 70215

S73-24213-24228 B&W
S73-15706-15712 mug, color
S73-15707 broken surface, both
S73-31668-31669
S76-21651 exploded parts
S73-31175-31179
S73-31664-31670
S74-24789
S75-24751
S79-26738-26740
S89-34488-34501

Table 1. Chemical composition of 70215.

reference	LSPET73	Rhodes74		Wiesmann75 Shih 75		Wanke75		Duncan74		Rose74		Masuda74		Dickinson89			Brunfeldt74	
weight																		
SiO2 %	37.19	38.46	(a)			38.3	(c)	37.91	(a)	37.62	(d)							
TiO2	13.14	12.48	(a)	14.5	(b)	12.53	(c)	13.08	(a)	13.2	(d)						13.08	(d)
Al2O3	8.67	9.01	(a)			8.71	(c)	8.86	(a)	8.79	(d)						9.11	(d)
FeO	19.62	19.46	(a)			19.94	(c)	19.96	(a)	19.22	(d)			16.2	20.1	(c)	19.09	(d)
MnO	0.28	0.29	(a)			0.25	(c)	0.264	(a)	0.27	(d)						0.27	(d)
MgO	8.52	7.91	(a)			8.32	(c)	7.99	(a)	9.34	(d)						7.47	(d)
CaO	10.43	10.94	(a)			10.63	(c)	10.77	(a)	10.82	(d)			12.9	13.3	(c)	10.92	(d)
Na2O	0.32	0.42	(a)			0.37	(c)	0.38	(a)	0.31	(d)			0.34	0.39	(c)	0.43	(d)
K2O	0.04	0.05	(a)	0.0435	(b)	0.045	(c)	0.041	(a)	0.08	(d)						0.05	(d)
P2O5	0.09	0.1	(a)			0.1	(c)	0.114	(a)	0.07	(d)							
S %	0.18	0.17	(a)			0.162	(c)	0.188	(a)									
sum																		
Sc ppm						85.9	(c)			92	(d)			77	88	(c)	89	(d)
V								50	(a)	64	(d)			*349*	*320*	(c)	117	(d)
Cr	2874	2668	(a)	3030	(b)	2710	(c)	2949	(a)	2805	(d)			2400	2300	(c)	2510	(d)
Co						21.3	(c)	23	(a)	33	(d)			15	22	(c)	20.4	(d)
Ni	2	4	(a)					<3	(a)	1	(d)						<10	(d)
Cu						6.4	(c)	<3	(a)	*22*	(d)						4.2	(d)
Zn	5	6	(a)			3	(c)	<2	(a)	4	(d)				59	(c)	2	(d)
Ga						3.56	(c)			6.3	(d)			20		(c)	3.1	(d)
Ge ppb														2.2	2.4	(c)		
As						46	(c)											
Se						0.17	(c)											
Rb	0.2	0.9	(a)	0.356	(b)	0.36	(c)	1	(a)	1	(d)						0.3	(d)
Sr	121	123	(a)	121	(b)	143	(c)	122	(a)	170	(d)						127	(d)
Y	75	69	(a)			58	(c)	63.6	(a)	73	(d)							
Zr	183	185	(a)			176	(c)	192	(a)	223	(d)							
Nb	20	21	(a)			18	(c)	20.8	(a)	20	(d)							
Mo																		
Ru																		
Rh																		
Pd ppb																		
Ag ppb																		
Cd ppb																		
In ppb																		
Sn ppb																		
Sb ppb																		
Te ppb																		
Cs ppm						0.013	(c)										0.02	(d)
Ba				56.9	(b)	59	(c)	77	(a)	*475*	(d)	61.8	(b)	47	65	(c)	48	(d)
La				5.22	(b)	5.54	(c)					5.35	(b)	4.7	5.8	(c)	4.96	(d)
Ce				16.5	(b)	19.6	(c)					17.3	(b)	13	17	(c)	11.3	(d)
Pr						3	(c)											
Nd				16.7	(b)	19	(c)					17	(b)	22		(c)		
Sm				6.69	(b)	6.7	(c)					6.98	(b)	6	6.9	(c)	6.78	(d)
Eu				1.37	(b)	1.4	(c)					1.45	(b)	1.3	1.4	(c)	1.4	(d)
Gd				10.4	(b)	9.1	(c)					10.3	(b)					
Tb						1.8	(c)							1.7	2	(c)	1.66	(d)
Dy				12.2	(b)	11.5	(c)					12.7	(b)				12.5	(d)
Ho						2.5	(c)											
Er				7.4	(b)	7.2	(c)					7.91	(b)	*0.62*		(c)		
Tm														1.4		(c)		
Yb				7.04	(b)	6.97	(c)			5	(d)	7.45	(b)	6.7	7.2	(c)	5.9	(d)
Lu				1.03	(b)	1.06	(c)					1.07	(b)	1.1	1.2	(c)	1.11	(d)
Hf						6.33	(c)							7.6	6.4	(c)	8.3	(d)
Ta						1.55	(c)							1.5	1.6	(c)	1.6	(d)
W ppb						86	(c)										75	(d)
Re ppb																		
Os ppb																		
Ir ppb																		
Pt ppb																		
Au ppb						0.3	(c)											
Th ppm						0.34	(c)							0.38	0.39	(c)	0.21	(d)
U ppm				0.13	(b)	0.091	(c)										0.072	(d)

technique: (a) XRF, (b) idms, (c) INAA, RNAA, (d) combined

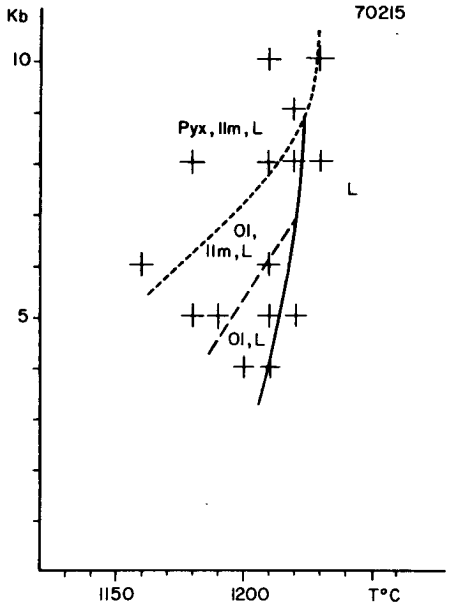

Figure 10: High pressure phase diagram for 70215 (from Kesson 1975).

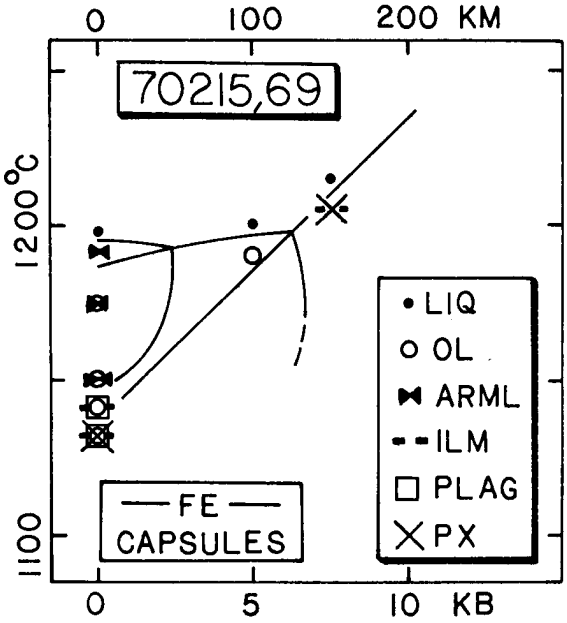

Figure 11: High pressure phase diagram for 70215 (from Walker et al. 1976).

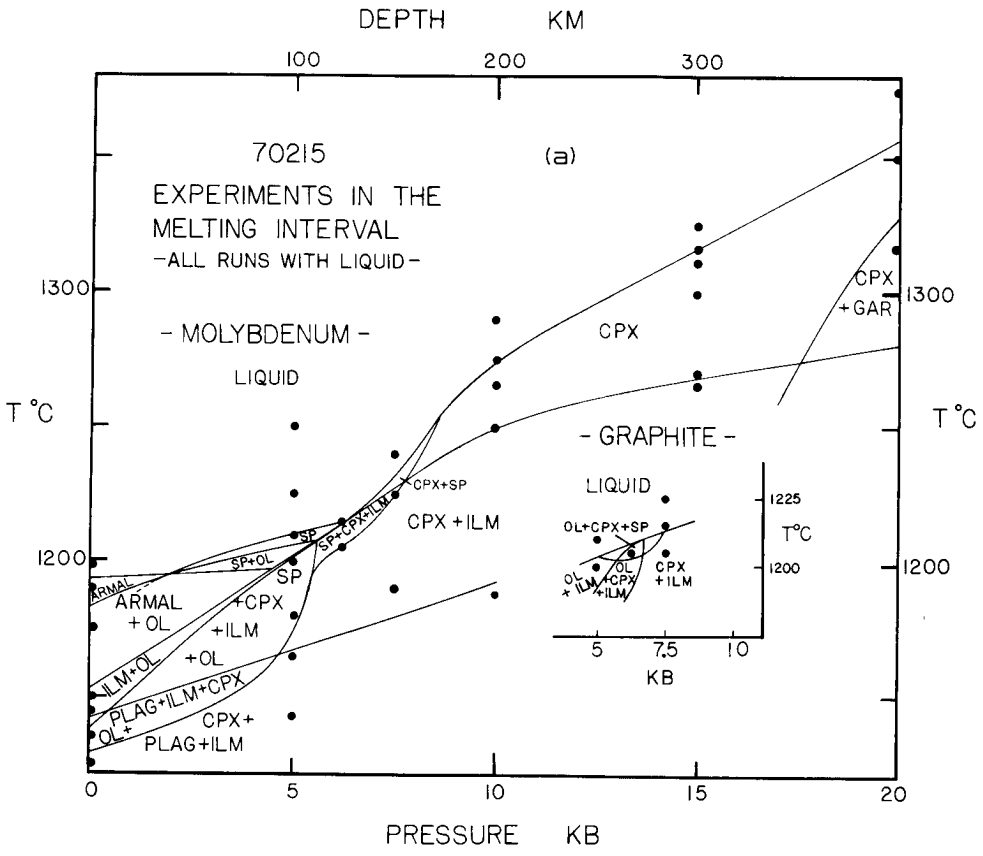

Figure 12: High pressure phase diagram for basalt 70215 determined in Mo and graphite capsules showing that a liquid of 70215 composition is "multiply saturated" at about 150 km depth on the moon (from Longhi et al. 1974).

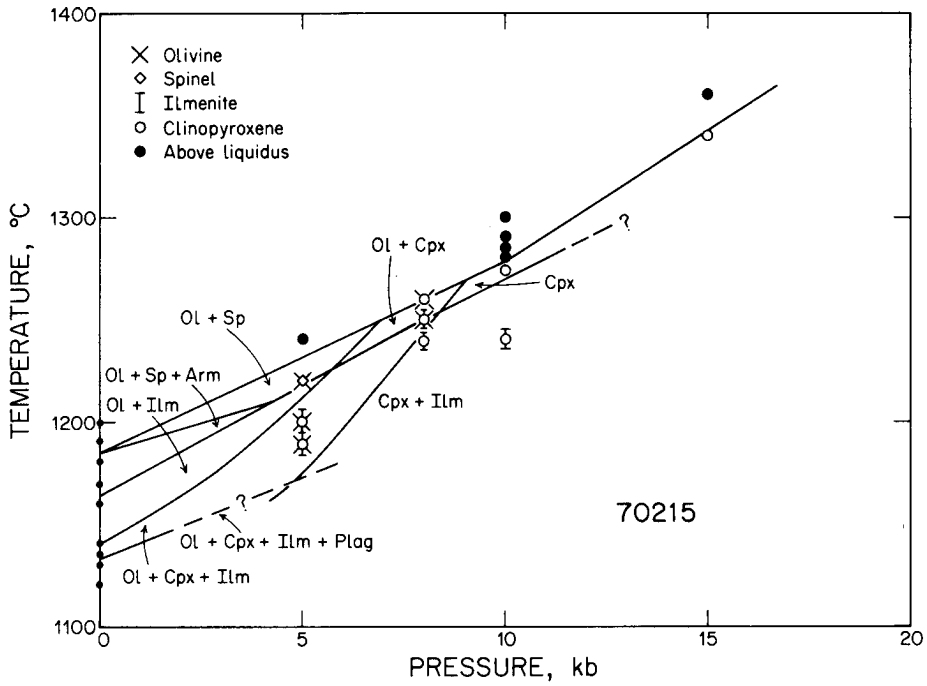

Figure 13: Experimental phase diagram showing mutiple satuation (without ilmenite) at about 8 kbar (from Green et al. 1975).

Figure 14: Photo of 70215 illustrating zap pits. Scale and cube are in cm. NASA photo # S73-15710.

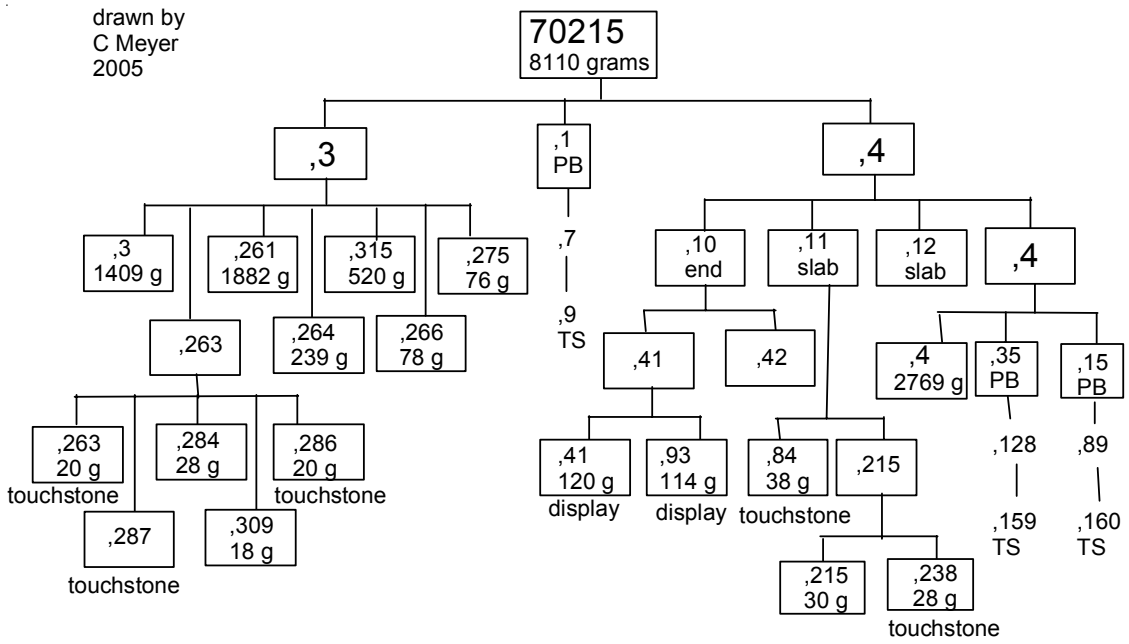

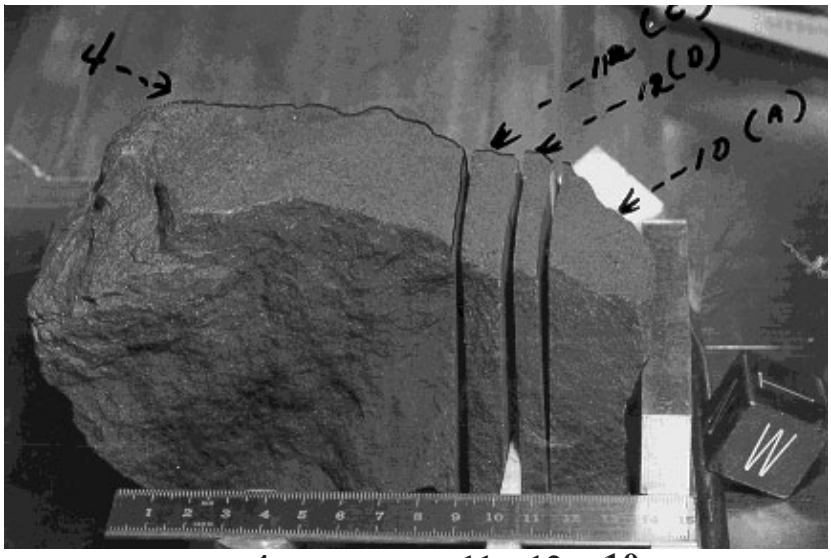

,4 ,11 ,12 ,10

Figure 15: First two slabs (,11 and ,12) and end piece (,10) cut from 70215,4 (picture from data pack). Cube is 1 inch. NASA # S76-21651.

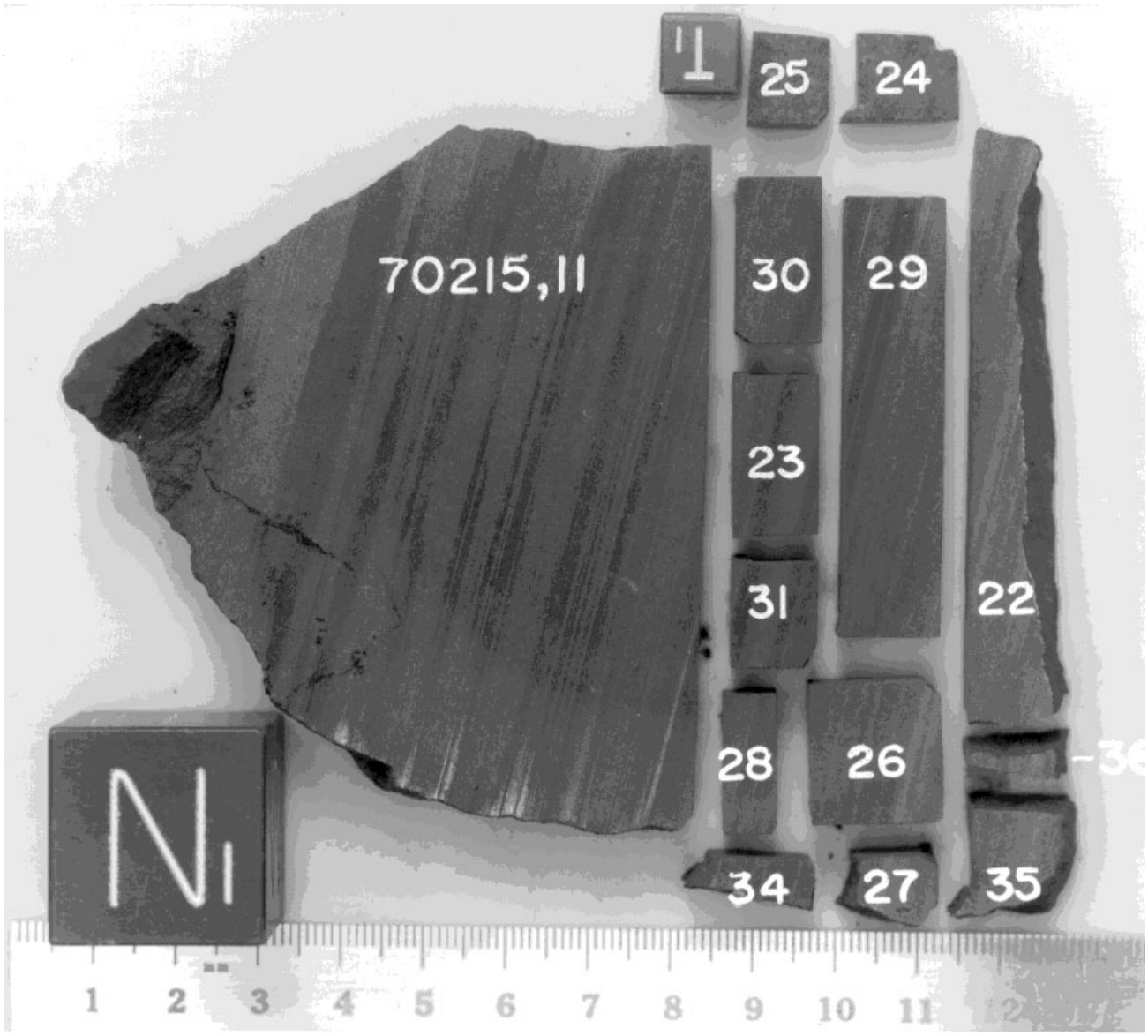


70215,12
,14
21
37
38
13
18
19
15
17
16
N1
mm
1 2 3 4 5 6 7 8 9 10 11

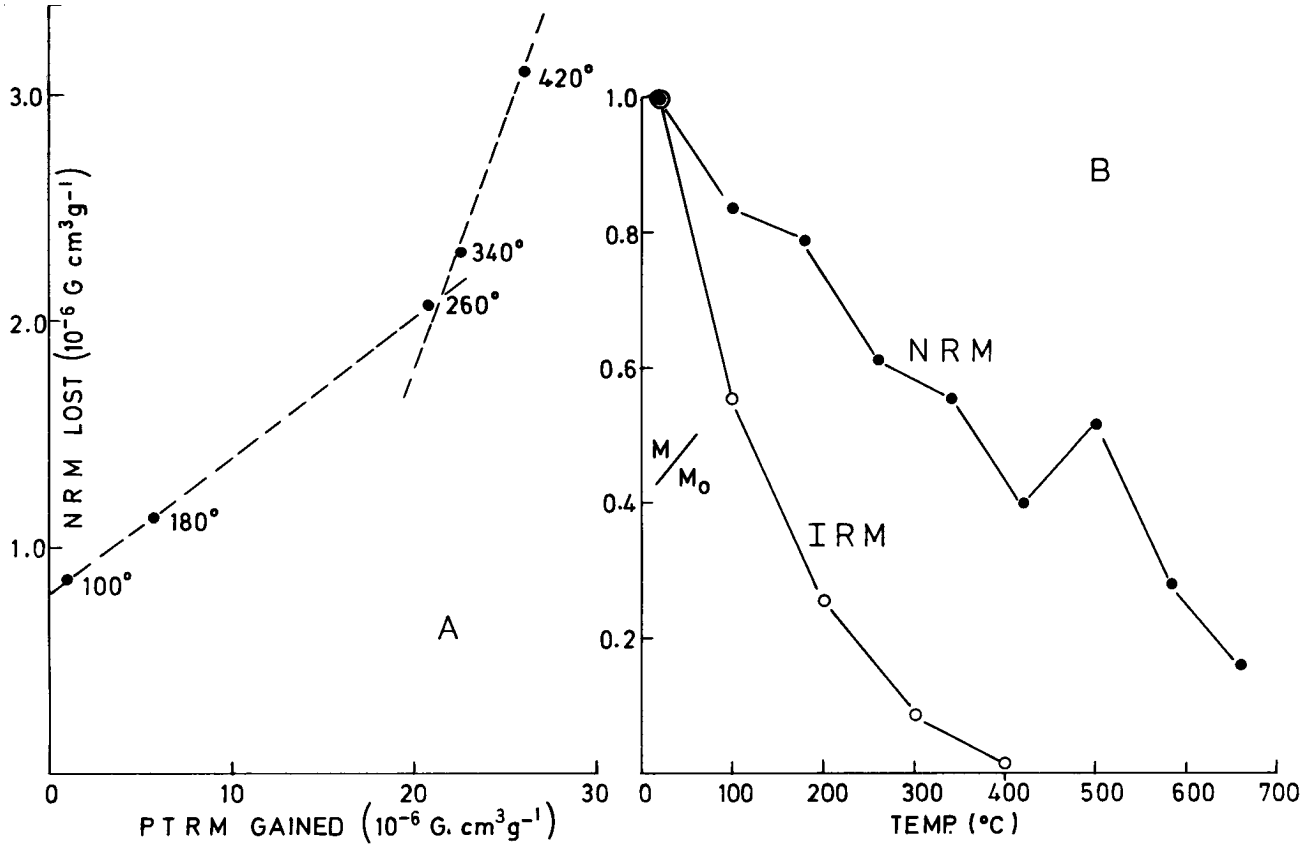

Fig. 8. Thellier determination of ancient field intensity (A) and thermal demagnetization of NRM and IRM acquired in 30 Oe(B) for 70215,45.

Figure 18: Two figures out of Stephenson et al. (1974) pertaining to remanent magnetization of 70215.

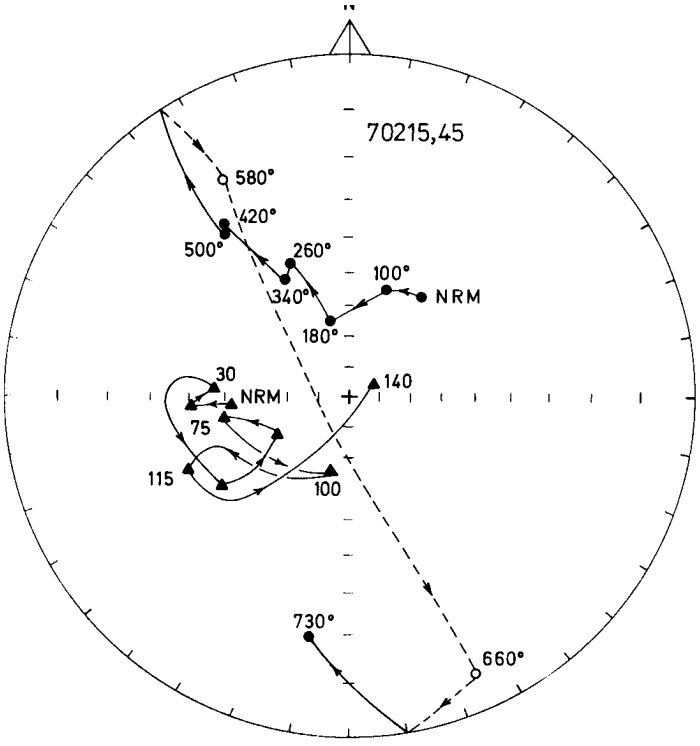

Fig. 7. AF and thermal demagnetization of chips from 70215,45. ● Thermal demagnetization; ▲ AF demagnetization.